Am J Transl Res 2026;18(1):826-841
www.ajtr.org /ISSN:1943-8141/AJTR0169710

Original Article

Dihydroartemisinin attenuates pemphigus vulgaris by regulating Dsg3 and the TLR9/NF-κB pathway

Yu Cui[1], Shuxia Song[2], Yi Cheng[1], Caixia Hu[1], Molin Yang[1], Wenqing Wang[1]

[1]*Department of Dermatology, The Fourth Hospital of Hebei Medical University, Shijiazhuang, Hebei, China;*
[2]*Department of Immunology, Hebei Medical University, Shijiazhuang, Hebei, China*

Received November 1, 2025; Accepted January 5, 2026; Epub January 25, 2026; Published January 30, 2026

Abstract: Objective: To evaluate the therapeutic efficacy of dihydroartemisinin (DHA) in pemphigus vulgaris (PV). Methods: Based on network pharmacology analysis, the TLR9/NF-κB signaling axis was selected as the primary pathway of interest. Skin specimens were first validated using immunohistochemistry. Subsequently, HaCaT cells were incubated. Desmoglein 3 (Dsg3) expression was detected using immunofluorescence staining. Cell viability was evaluated using MTS assay. The expression levels of TLR9, TRAF6, MyD88, p-NF-κB p65, MMP-9, and ADAM10 in HaCaT cells treated with control IgG (C-IgG), PV-IgG, and DHA were then examined by western blotting. Finally, these indicators were evaluated in Kunming mice. The results demonstrated that DHA suppressed PV-IgG - induced Dsg3 internalization and depletion. PV-IgG appeared to activate the NF-κB pathway through TLR9/TRAF6 signaling, while DHA effectively inhibited this effect. Moreover, DHA downregulated the expression of ADAM10 and MMP-9, critical proteases involved in the pathogenesis of PV.

Keywords: Pemphigus vulgaris, Dsg3, TLR9, TRAF6, p-NF-κB p65, MMP-9, ADAM10, dihydroartemisinin, network pharmacology

Introduction

Pemphigus, as an autoimmune mucocutaneous bullosa disease, poses a serious threat to human health. The disease primarily affects individuals aged 45-60 years [1]. Pemphigus is classified into five types: pemphigus vulgaris (PV), pemphigus foliaceus (PF), paraneoplastic pemphigus, pemphigus herpetiformis, and IgA pemphigus [2]. Among them, PV is the most common and severe form and can even be life-threatening if not properly managed [3]. Epidemiological studies have reported that the prevalence of PV is approximately 95 per million people, with an annual incidence of about 2.83 per million [4, 5]. The classical clinical manifestations of PV include painful oral mucosa erosions, flabby blisters, and erosive crusting on apparently normal or erythematous skin [6]. PV is primarily driven by autoantibodies against desmoglein 1 and 3, leading to impaired keratinocyte adhesion, and is further aggravated by activation of epidermal growth factor receptor (EGFR) and nuclear factor kappa-B (NF-κB) signaling as well as $CD4^+$ T cell - mediated immune responses [6, 21].

Systemic corticosteroids remain the first-line treatment for PV [7]. However, long-term glucocorticoid therapy is associated with a wide range of side effects, including peptic ulcer disease, osteoporosis, hypertension, hyperglycemia, hypokalemia, psychiatric disorders, adrenal crisis, immunosuppression, and infection [8], resulting in unfavorable patient outcomes and even death [9, 10]. Therefore, there is an urgent need to identify alternative therapeutic drugs with fewer side effects.

Artemisinin, isolated from *Artemisia annua L.*, is a well-established antimalaria agent. In 2015, Chinese scientist Tu Youyou was awarded the Nobel Prize in Physiology or Medicine for the discovery of artemisinin and its antimalarial efficacy [11, 12]. Dihydroartemisinin (DHA), a first-generation derivative and the major active metabolite of artemisinin, exhibits superior anti-malarial efficacy and bioavailability [13] and has recently emerged as a promis-

https://doi.org/10.62347/TZCU8488

ing immunomodulator. Preclinical studies demonstrate DHA's therapeutic potential in autoimmune and inflammatory diseases [16-18], including amelioration of systemic lupus erythematosus in BXSB mice [14], attenuation of psoriatic skin inflammation by targeting $CD8^+$ T-cell memory [15], and mitigation of collagen-induced arthritis by restoring Treg/Th17 balance [19]. Mechanistically, DHA suppresses B-cell activation and antibody production [58], inhibits TLR4-dependent NF-κB signaling [59, 60], and downregulates proinflammatory cytokines such as interleukin-6 (IL-6) and IL-1β [61].

Given the immunomodulatory properties of DHA and the critical role of NF-κB signaling in PV pathogenesis, we hypothesized that DHA may alleviate PV by regulating Desmoglein 3 (Dsg3) and NF-κB-related pathways. To validate this hypothesis, we employed an integrated approach combining network pharmacology analysis to identify common DHA-PV targets and key pathways with clinical sample validation, *in vitro* HaCaT cell experiments, and *in vivo* Kunming mouse models. This multi-tiered approach aimed to clarify DHA's therapeutic effect in PV and to clarify its underlying mechanism, thereby providing a scientific basis for developing novel PV treatments.

Materials and methods

Network pharmacological analysis

Targets of DHA were retrieved from the GeneCards database (https://www.genecards.org/), the HERB database (http://herb.ac.cn/), and the SwissTargetPrediction database (http://www.swisstargetprediction.ch/). PV-related genes were obtained from the Online Mendelian Inheritance in Man (OMIM; https://omim.org/), GeneCards, and PharmGkb (https://www.pharmgkb.org/) databases. Protein-protein interaction (PPI) analysis was performed using STRING database (https://cn.string-db.org/), and all network diagrams were visualized using Cytoscape software (version 3.8.0).

Gene Ontology (GO) and Kyoto Encyclopedia of Genes and Genomes (KEGG) enrichment analysis

GO and KEGG enrichment analyses were conducted using the R language software. The *GSEABase* package, *GSVA* package, *clusterProfiler* package, and *org.Hs.eg.db* package were used for enrichment analysis. The *ggplot2* package and the *ggpubr* package were used for visualization.

Case selection

Patients included in this study met the following criteria: (1) age between 18 and 75 years; (2) clinician-confirmed PV diagnosis based on typical clinical manifestations (blisters or erosions), histopathological findings from skin or mucosal biopsies, and serological detection of desmoglein autoantibodies by enzyme-linked immunosorbent assay (ELISA) [20]. Exclusion criteria included: (1) a history of glucocorticoid or biological agent use within the past month; (2) presence with other autoimmune diseases, malignant tumors, or infectious diseases. All patients provided written informed consent, and the study was approved by the Ethics Committee of the Fourth Hospital of Hebei Medical University (2022KY397).

Control biopsies were obtained from patients undergoing routine surgery (n = 9, normal human skin). Control serum was obtained from people undergoing routine medical examinations without significant abnormalities. All these donors provided informed consent.

Hematoxylin and Eosin (H&E) staining

After rapid excision, donor skin specimens were fixed, paraffinized, and sectioned into 5 μm-thick slices. Samples were deparaffinized using two rounds of xylene treatment (10 min each), followed by rehydration with two rounds of absolute ethanol (5 min each) and rinsing with tap water. H&E staining was performed to observe tissue morphology.

Immunohistochemistry (IHC)

Skin sections were incubated overnight at 4°C with primary antibodies against toll-like receptor 9 (TLR9), myeloid differentiation primary response 88 (MyD88), tumor necrosis factor receptor-associated factor 6 (TRAF6), phosphorylated-NF-κB p65 (p-NF-κB p65), a disintegrin and metalloproteinase 10 (ADAM-10), matrix metalloproteinase-9 (MMP-9), and Dsg3 (1:100 dilution). The sections were then incubated with a biotinylated secondary anti-

rabbit IgG antibody at a 1:500 dilution, and the signal was visualized by DAB staining. Finally, the sections were examined and imaged under a light microscope. Histological assessments were independently performed by three investigators who were blinded to the study groups.

Purification of PV IgG

Peripheral blood samples (50 ml) were collected from clinically diagnosed patients with PV, and the serum was separated by conventional methods. Serum IgG was purified by DEAE-Sephadex A-50 ion exchange chromatography. To obtain high concentration IgG, serum samples were obtained from a patient on plasmapheresis. The processed DEAE-Sephadex A-50 was packed into a chromatography column equilibrated until the pH and conductivity of the eluate were consistent with those of the buffer. The serum samples were slowly loaded onto the column, and fractions were collected during elution. The collected fractions were concentrated and quantified for protein content. Finally, the purified PV-IgG was prepared at a concentration of 4 mg/ml and stored for subsequent use.

Immunofluorescence (IF) staining

HaCaT cells were randomly divided into three groups: negative control group, control IgG group (C-IgG; normal human serum IgG) group, and PV-IgG group. Cells were incubated with PBS, C-IgG (300 μg/ml), or PV-IgG (300 μg/ml), respectively, for 4 hours. Then, the C-IgG group and the PV-IgG group were further subdivided into two subgroups and treated with DHA (0 or 25 μg/ml). Cells were routinely cultured for an additional 24 hours under standard conditions. Subsequently, cells were incubated with anti-human Dsg3 antibody diluted 1:200 in goat serum, followed by incubation with green fluorescent-labeled secondary goat anti-rabbit IgG antibody diluted 1:100. Finally, a sealing solution containing anti-fluorescence quencher and DAPI mixture was applied, and the cells were observed under a fluorescence microscope.

Cell assays

Cell culture: HaCaT cells, purchased from HyCyte™, were cultured in DMEM supplemented with fetal bovine serum at 37°C under 5% CO_2. Once the cells reached around 80-90% confluence, they were detached using 0.25% trypsin-EDTA, and digestion was stopped by adding complete medium. Cells were then collected by centrifugation at 1,500 rpm for 3 minutes and passaged at a ratio of 1:2-1:4. Only cells in the logarithmic growth phase were used for subsequent experiments.

Treatment of HaCaT cells: HaCaT cells were cultured in 6-well plates at a density of 10^5 cells per well. After cells adhesion, PV-IgG at concentrations of 150, 300, 450 or 600 μg/ml was added. Cells treated with same amount of C-IgG served as negative controls. Cells were incubated for 48 hours at 37°C in an incubator containing 5% CO_2 saturated water vapor. The culture medium was then removed, and cells were washed once with PBS, harvested, and total cellular protein was extracted.

Effects of DHA on HaCaT cell viability: HaCaT cells in the logarithmic growth phase were collected, counted, and adjusted to 1×10^5/ml. Cells were seeded into 96-well plates at 1×10^4 per well and cultured for 8 hours to allow cell adhesion. DHA was added to achieve final concentrations of 0, 15, 25, 50, 75, 100 or 125 μg/ml, and fresh culture medium was supplemented to a final volume of 200 μl per well. Cells were further incubated for 24 or 48 hours to observe the effects of DHA on HaCaT cell viability. A volume of 15 μl of MTS was added to each well 1.5 hours before the end of incubation. The supernatant was subsequently collected and centrifuged at 1,000 rpm at room temperature for 10 minutes. The absorbance value at 570 nm was measured using a microplate reader.

Effects of DHA on signal protein expression in HaCat cells: HaCaT cells in the logarithmic growth phase were seeded and routinely cultured for 8 hours until adherence. Then, PV-IgG or C-IgG was added at an ultimate concentration of 300 μg/ml to prepare the PV cell model. Meanwhile, the cells were divided into 3 groups: the control group, the low-dose DHA treatment group, and the high-dose DHA treatment group. DHA was added at final concentrations of 0, 15 or 30 μg/ml, respectively, while the control group was treated with PBS containing equivalent volume of DMSO. Cells were cultivated for an additional 24 h, and the pro-

tein expression levels were detected by Western blotting.

Animal experiments

All in vivo experiments were approved by the Animal Ethics Committee of the Fourth Hospital of Hebei Medical University (IACUC-4th Hos Hebmu-20240201). Kunming mice (2-3 days old), all purchased from Beijing Weitong Lihua Experimental Animal Technology Co., Ltd., were randomly divided into the following groups: normal control group (NC), C-IgG group, C-IgG + DHA group, PV-IgG group, and PV-IgG + DHA group. Mice in C-IgG and PV-IgG groups were administered with IgG (0.5 mg) on day 1, with a second injection administered 6 hours later, then on days 2 and 3, respectively, with a total IgG dose of 2.0 mg. Mice in DHA group were treated with DHA (10 μg) on day 1. Three hours after the first DHA administration, 0.5 mg of normal IgG or PV-IgG was administered, followed by a second IgG injection (0.5 mg) 6 h after the first dose. The mice were treated with 10 μg DHA on day 2 and day 3, followed by 0.5 mg IgG 3h later. In total, mice received 20 μg DHA and 2.0 mg IgG, with both substances delivered via intraperitoneal injection. Mice were euthanized 24 hours after the last IgG administration by gradual CO_2 inhalation, and skin specimens were subsequently collected for H&E staining, IHC, immunofluorescence and western blot analyses.

Statistical analysis

SPSS 24.0 software was used for statistical analysis. All experimental data were expressed as means ± standard deviation (SD) of three independent experiments. One-way analysis of variance and independent-sample t-test were used for statistical analysis. A P value < 0.05 was considered statistically significant.

Results

The TLR9/NF-κB pathway and its downstream effector proteins were upregulated in PV process

In this study, 570 active components of DHA were identified from the GeneCards, HERB, and SwissTargetPrediction database. PV-related targets were obtained through OMIM, GeneCards, and PharmGkb databases using the keyword “pemphigus vulgaris”. A total of 217 targets were identified. By intersecting PV- and DHA-related targets using a Venn diagram, a total of 37 common targets were identified, as shown in **Figure 1A**.

These intersection targets were imported into the STRING database, and the PPI network diagram was constructed using Cytoscape 3.8.0 software, as shown in **Figure 1B**, **1C**. GO and KEGG enrichment analyses were performed on the 37 common targets using R 4.0.3 software (restricted species: Homo sapiens; P < 0.05). A total of 1,346 GO enriched terms were enriched. Of these, 1,152 were biological process terms, mainly related to responses to molecules of bacterial origin, lipopolysaccharide, tumor necrosis factor, cellular response to external stimuli, and positive regulation of cytokine production. Additionally, a total of 85 cellular component terms were identified, mainly involving fibronectin 1-rich particles and their lumens, vesicle lumens, membrane rafts, and membrane microdomains. Additionally, 109 molecular function items were enriched, mainly related to cysteine endopeptidase activity involved in the transduction of apoptotic signaling pathways, endopeptidase activity, cysteine-type endopeptidase activity involved in the apoptotic process, phospholipase activator activity, and lipase activator activity. Furthermore, a total of 115 enriched pathways were identified in KEGG analysis, predominantly related to lipid and atherosclerosis, TNF signaling pathway, kaposi’s sarcoma-associated herpesvirus infection, AGE-RAGE signaling pathway associated with diabetic complications, and prostate cancer. According to P values, the top 10 GO terms and the top 20 KEGG pathways were selected for further analysis (**Tables 1**-**4**). Diagram of the disease-drug-pathway-target network and the bubble chart were generated, as shown in **Figure 2**.

Histopathological examination of PV samples revealed suprabasal acantholysis, leading to intraepidermal cleft or blister formation, with acantholytic keratinocytes observed within the blister cavities (**Figure 3A**, **3B**). In normal epidermal cells, TLR9, Myd88, and TRAF6 were mainly localized in the cytoplasm. Compared with control samples, PV samples demonstrated markedly increased expression of these three proteins. Phosphorylated NF-κB p65 was distributed in both cytoplasmic and nuclear

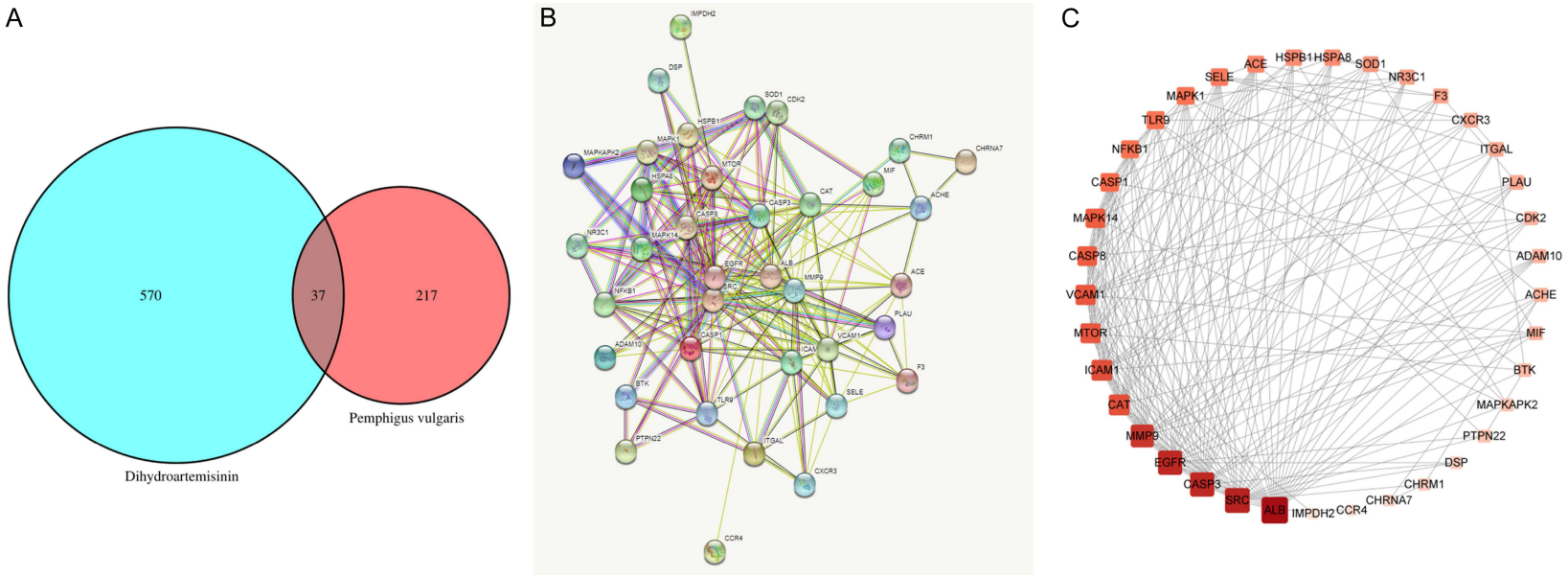

Figure 1. Network pharmacology analysis of therapeutic targets of DHA in PV. A. Venn diagram illustrating the intersecting targets between DHA- and PV- associated genes; B. Protein-protein interaction (PPI) map constructed using the STRING database; C. Topological representation of the PPI network generated with Cytoscape 3.8.0. Notes: DHA, dihydroartemisinin; PV, pemphigus vulgaris.

Table 1. Top 10 GO terms enriched in biological process (BP)

ID	Description	p.adjust	GeneID
GO:0002237	response to molecules of bacterial origin	0.00000000	PTPN22/MAPK14/ICAM1/SELE/CASP3/MAPK1/SRC/NFKB1/VCAM1/TLR9/MAPKAPK2/CASP1/CASP8
GO:0032496	response to lipopolysaccharide	0.00000000	PTPN22/MAPK14/ICAM1/SELE/CASP3/MAPK1/SRC/NFKB1/VCAM1/MAPKAPK2/CASP1/CASP8
GO:0034612	response to tumor necrosis factor	0.00000003	MAPK14/ICAM1/SELE/CASP3/MAPK1/NFKB1/ADAM10/VCAM1/CASP1/CASP8
GO:0071496	cellular response to external stimulus	0.00000024	EGFR/ICAM1/MTOR/MAPK1/NFKB1/VCAM1/CASP1/CASP8/HSPA8/ALB
GO:0001819	positive regulation of cytokine production	0.00000043	PTPN22/MAPK14/SOD1/SRC/HSPB1/MIF/TLR9/MAPKAPK2/CASP1/CASP8/F3
GO:0050900	leukocyte migration	0.00000062	ICAM1/SELE/MAPK1/MMP-9/SRC/ADAM10/MIF/CXCR3/VCAM1/ITGAL
GO:0050727	regulation of inflammatory response	0.00000082	BTK/EGFR/MAPK14/SELE/SOD1/MMP-9/SRC/NFKB1/TLR9/CASP1
GO:0001666	response to hypoxia	0.00000174	PLAU/CAT/ICAM1/MTOR/CASP3/SRC/VCAM1/CASP1/CHRNA7
GO:0070661	leukocyte proliferation	0.00000197	BTK/IMPDH2/PTPN22/CASP3/MAPK1/ACE/MIF/VCAM1/TLR9
GO:0036293	response to decreased oxygen levels	0.00000197	PLAU/CAT/ICAM1/MTOR/CASP3/SRC/VCAM1/CASP1/CHRNA7

Table 2. Top 10 GO terms enrich in cellular component (CC)

ID	Description	p.adjust	Gene ID
GO:0101002	ficolin-1-rich granule	0.00000029	IMPDH2/DSP/CAT/MAPK14/MAPK1/MMP-9/MIF/HSPA8
GO:1904813	ficolin-1-rich granule lumen	0.00000029	IMPDH2/CAT/MAPK14/MAPK1/MMP-9/MIF/HSPA8
GO:0031983	vesicle lumen	0.00000035	IMPDH2/CAT/EGFR/MAPK14/MAPK1/NFKB1/MIF/HSPA8/ALB
GO:0045121	membrane raft	0.00000035	BTK/EGFR/ICAM1/SELE/CASP3/MAPK1/SRC/CASP8/CHRNA7
GO:0098857	membrane microdomain	0.00000035	BTK/EGFR/ICAM1/SELE/CASP3/MAPK1/SRC/CASP8/CHRNA7
GO:0005925	focal adhesion	0.00000193	PLAU/CAT/EGFR/ICAM1/MAPK1/SRC/HSPB1/ADAM10/HSPA8
GO:0030055	cell-substrate junction	0.00000193	PLAU/CAT/EGFR/ICAM1/MAPK1/SRC/HSPB1/ADAM10/HSPA8
GO:0034774	secretory granule lumen	0.00000282	IMPDH2/CAT/MAPK14/MAPK1/NFKB1/MIF/HSPA8/ALB
GO:0060205	cytoplasmic vesicle lumen	0.00000282	IMPDH2/CAT/MAPK14/MAPK1/NFKB1/MIF/HSPA8/ALB
GO:0009897	external side of plasma membrane	0.00022506	ICAM1/SELE/ACE/CCR4/CXCR3/VCAM1/F3

Table 3. Top 10 GO terms enriched in molecular function (MF)

ID	Description	p.adjust	Gene ID
GO:0097199	cysteine-type endopeptidase activity involved in apoptotic signaling pathway	0.00021013	CASP3/CASP1/CASP8
GO:0004175	endopeptidase activity	0.00021136	PLAU/CASP3/MMP-9/ACE/ADAM10/CASP1/CASP8/F3
GO:0097153	cysteine-type endopeptidase activity involved in apoptotic process	0.00024312	CASP3/CASP1/CASP8
GO:0016004	phospholipase activator activity	0.00024312	BTK/CASP3/SRC
GO:0060229	lipase activator activity	0.00028262	BTK/CASP3/SRC
GO:0005178	integrin binding	0.00038531	EGFR/ICAM1/SRC/ADAM10/VCAM1
GO:0043274	phospholipase binding	0.00049305	BTK/SELE/SRC
GO:0051019	mitogen-activated protein kinase binding	0.00049305	MAPK14/ACE/MAPKAPK2
GO:0017171	serine hydrolase activity	0.00110638	PLAU/MMP-9/ACE/ACHE/F3
GO:0004674	protein serine/threonine kinase activity	0.00260789	EGFR/MAPK14/MTOR/MAPK1/CDK2/MAPKAPK2

Table 4. Top 20 KEGG pathways

ID	Description	p.adjust	Gene ID
hsa05417	Lipid and atherosclerosis	0.0000000112	MAPK14/ICAM1/SELE/CASP3/MAPK1/MMP-9/SRC/NFKB1/VCAM1/CASP1/CASP8/HSPA8
hsa04668	TNF signaling pathway	0.0000000818	MAPK14/ICAM1/SELE/CASP3/MAPK1/MMP-9/NFKB1/VCAM1/CASP8
hsa05167	Kaposi sarcoma-associated herpesvirus infection	0.0000004141	MAPK14/ICAM1/MTOR/CASP3/MAPK1/SRC/NFKB1/CCR4/MAPKAPK2/CASP8
hsa04933	AGE-RAGE signaling pathway in diabetic complications	0.0000004141	MAPK14/ICAM1/SELE/CASP3/MAPK1/NFKB1/VCAM1/F3
hsa05215	Prostate cancer	0.0000064338	PLAU/EGFR/MTOR/MAPK1/MMP-9/NFKB1/CDK2
hsa04625	C-type lectin receptor signaling pathway	0.0000086736	MAPK14/MAPK1/SRC/NFKB1/MAPKAPK2/CASP1/CASP8
hsa05161	Hepatitis B	0.0000103671	MAPK14/CASP3/MAPK1/MMP-9/SRC/NFKB1/CDK2/CASP8
hsa05120	Epithelial cell signaling in Helicobacter pylori infection	0.0000120665	EGFR/MAPK14/CASP3/SRC/NFKB1/ADAM10
hsa05418	Fluid shear stress and atherosclerosis	0.0000311001	MAPK14/ICAM1/SELE/MMP-9/SRC/NFKB1/VCAM1
hsa05169	Epstein-Barr virus infection	0.0000311001	BTK/MAPK14/ICAM1/CASP3/NFKB1/CDK2/ITGAL/CASP8
hsa05235	PD-L1 expression and PD-1 checkpoint pathway in cancer	0.0000311001	EGFR/MAPK14/MTOR/MAPK1/NFKB1/TLR9
hsa05203	Viral carcinogenesis	0.0000311001	CASP3/MAPK1/SRC/NFKB1/CCR4/CDK2/MAPKAPK2/CASP8
hsa05205	Proteoglycans in cancer	0.0000311001	PLAU/EGFR/MAPK14/MTOR/CASP3/MAPK1/MMP-9/SRC
hsa05144	Malaria	0.0000311001	ICAM1/SELE/VCAM1/ITGAL/TLR9
hsa04657	IL-17 signaling pathway	0.0000370369	MAPK14/CASP3/MAPK1/MMP-9/NFKB1/CASP8
hsa01522	Endocrine resistance	0.0000443229	EGFR/MAPK14/MTOR/MAPK1/MMP-9/SRC
hsa05134	Legionellosis	0.0000471451	CASP3/NFKB1/CASP1/CASP8/HSPA8
hsa05163	Human cytomegalovirus infection	0.0000471451	EGFR/MAPK14/MTOR/CASP3/MAPK1/SRC/NFKB1/CASP8
hsa05142	Chagas disease	0.0000471451	MAPK14/MAPK1/ACE/NFKB1/TLR9/CASP8
hsa04370	VEGF signaling pathway	0.0000499906	MAPK14/MAPK1/SRC/HSPB1/MAPKAPK2

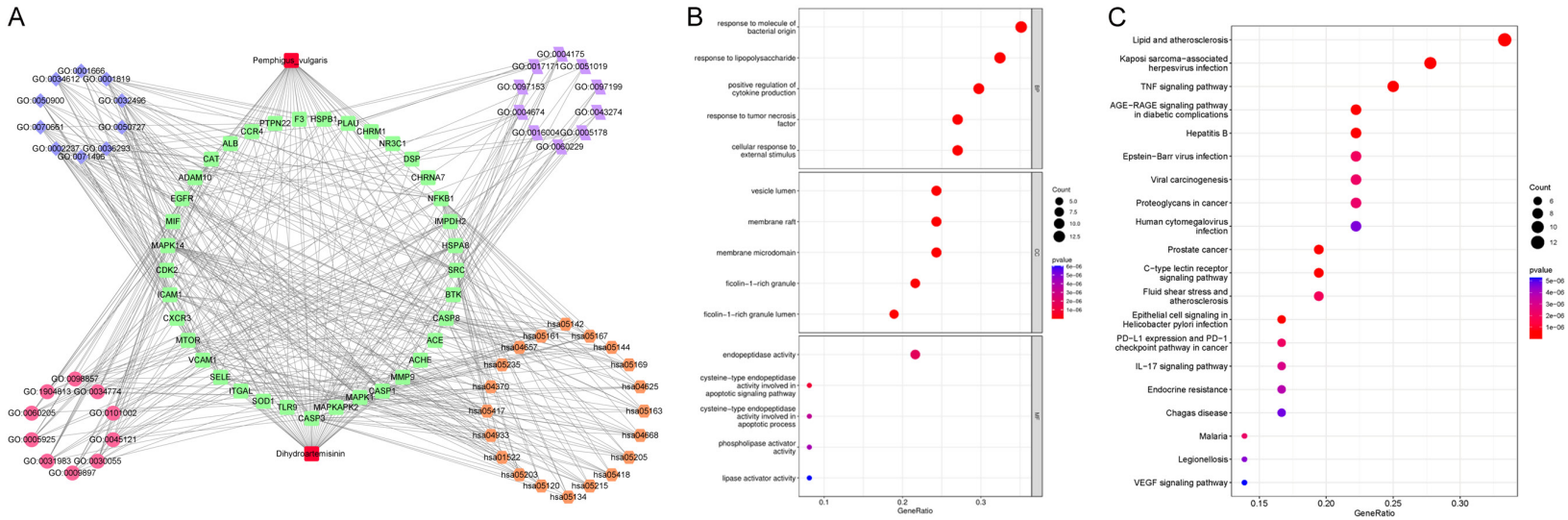

Figure 2. GO and KEGG enrichment analyses of common targets between DHA and PV. A. An integrated network depicting disease-drug-pathway-target relationships. Green rectangles represent 37 common targets, blue diamonds correspond to the 10 most significantly enriched biological process (BP) terms from GO analysis, pink circles denote the leading 10 cellular component (CC) terms, purple parallelograms identify the top molecular function (MF) terms, and orange hexagons signify the 20 highest-ranked KEGG pathways; B. Bar plots display the 5 most significantly overrepresented GO terms across BP, CC, and MF categories (**$P < 0.05$); C. The top 20 significantly enriched KEGG pathways ($P < 0.05$). Notes: DHA, dihydroartemisinin; PV, pemphigus vulgaris.

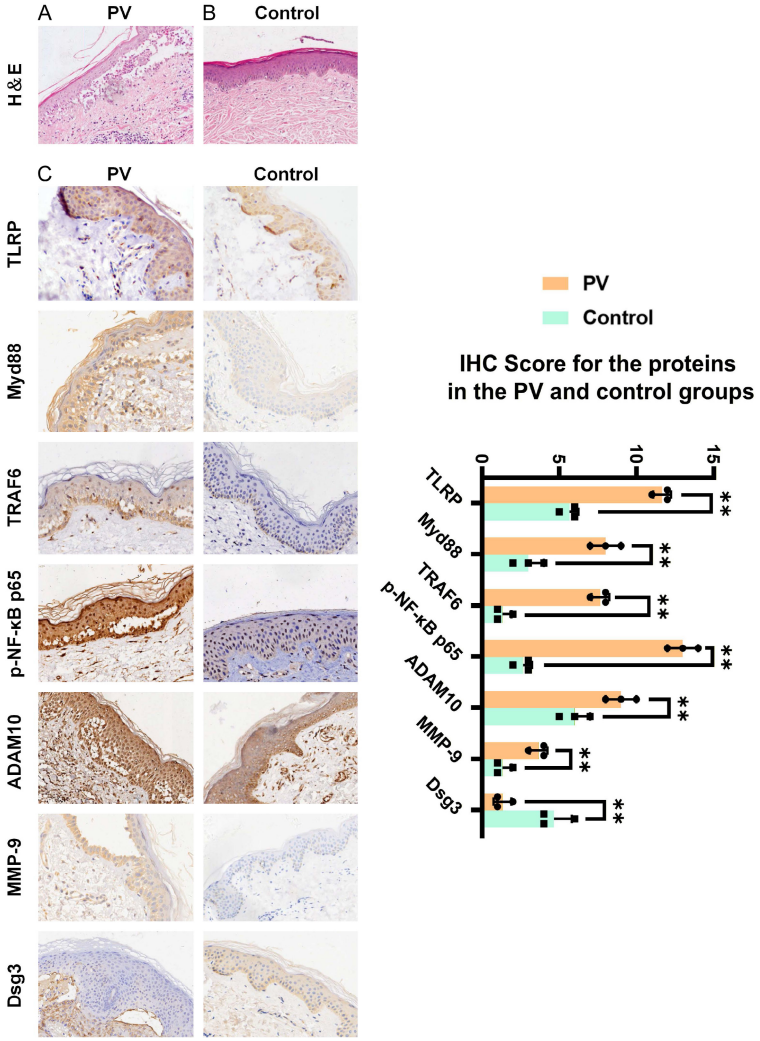

Figure 3. Histopathological and immunohistochemical analyses of PV and control tissues. A. Representative H&E-stained PV lesions (×200); B. Representative H&E-stained normal tissues (×200); C. Representative IHC staining for TLRP, Myd88, TRAF6, p-NF-κB p65, ADAM10, MMP-9, and Dsg3 in the PV and control tissues (×400). Notes: PV, pemphigus vulgaris; IHC, immunohistochemical (n = 3, **$P < 0.05$).

regions, and its levels were significantly higher in PV tissues. ADAM10 was detected in the cytoplasmic and membranous compartments, with expression also elevated in PV samples. Conversely, Dsg3, predominantly localized in the cell membrane, was notably reduced in PV epidermis. MMP-9, localized in the cytoplasm, showed significantly enhanced expression in PV compared with control samples (**Figure 3C**).

DHA inhibited PV-IgG-induced internalization and depletion of Dsg3 in keratinocytes

Total PV-IgG was isolated from the serum of PV patients by the DEAE-Sephadex A-50 method. Human keratinocyte HaCaT cells were cultured *in vitro* and treated with PBS, C-IgG, or PV-IgG for 24 hours. Immunofluorescence staining showed that Dsg3 was highly expressed in HaCaT cells and was mainly localized to the cell membrane. C-IgG didn't exert significant effects on the expression or localization of Dsg3. However, PV-IgG treatment resulted in notable redistribution of Dsg3 from membrane to intracellular compartments (**Figure 4**), indicating that PV-IgG can mediate the internalization and depletion of Dsg3. However, DHA treatment effectively attenuated this effect induced by PV-IgG.

DHA suppressed PV-IgG-induced TLR9/NF-κB signaling activation and down-regulated ADAM10/MMP-9 expression

HaCaT cells in the logarithmic growth phase were seeded into six-well plates (1×10^5 cells/well) and incubated with either PV-IgG at serial concentrations (150, 300, 450, and 600 μg/ml) or C-IgG for 48 h, with PBS as the blank control. Western blot analysis showed that C-IgG treatment did not notably alter the levels of

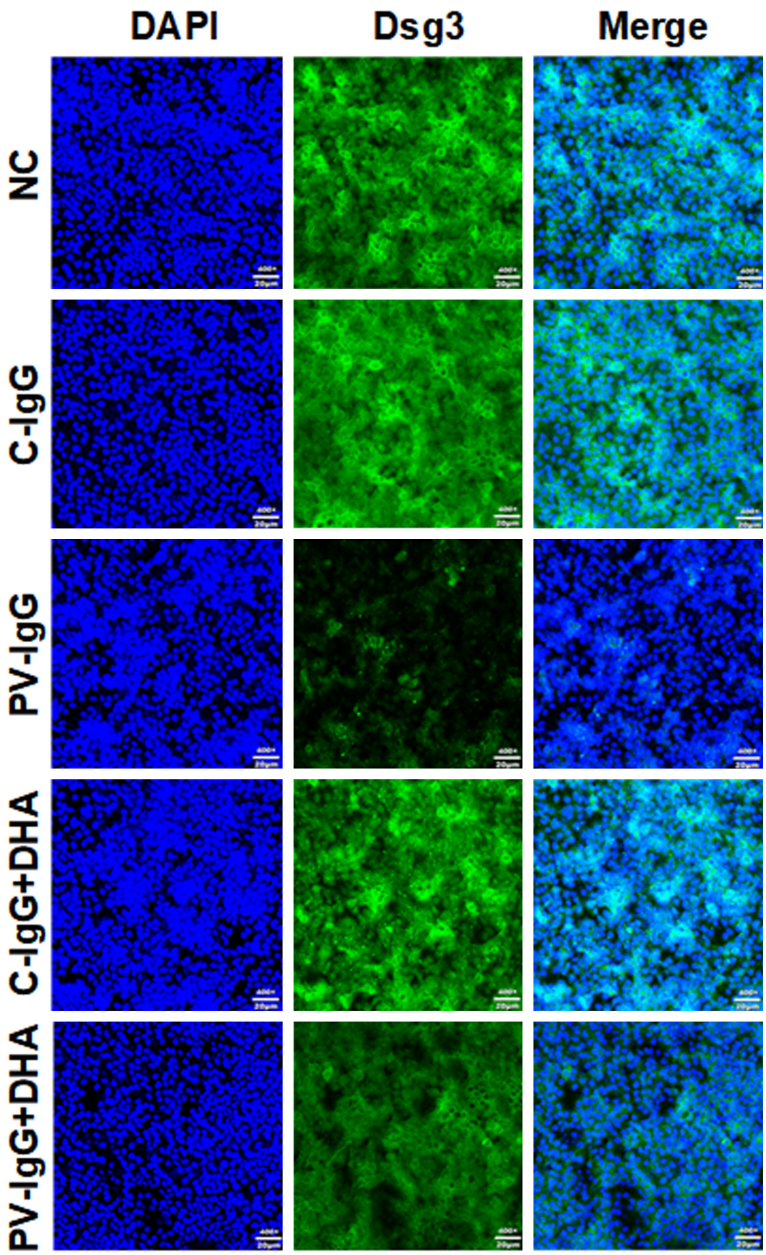

Figure 4. DHA inhibited PV-IgG-induced internalization and depletion of Dsg3 in HaCaT cells. Immunofluorescence staining revealed that PV-IgG induced pronounced internalization and depletion of membranous Dsg3, which was significantly suppressed upon DHA administration (×400). Notes: DHA, dihydroartemisinin; PV, pemphigus vulgaris; Dsg3, desmoglein 3.

TLR9, MyD88, TRAF6, or phosphorylated NF-κB p65 compared with controls, whereas PV-IgG induced a concentration-dependent increase in these proteins (**Figure 5A**).

The cytotoxicity of DHA was evaluated by MTS assay, revealing a dose- and time-dependent decrease in HaCaT cell viability following exposure to increasing DHA concentrations (0-125 μg/ml for 24 or 48 h) (**Figure 5B**). HaCaT cells pretreated with PV-IgG (300 μg/ml) exhibited significant upregulation of TLR9, TRAF6, and phosphorylated NF-κB p65, which was markedly reduced by DHA co-treatment in a dose-dependent manner.

Furthermore, PV-IgG stimulation (300 μg/ml, 24 h) was related to the upregulation of ADAM10 and MMP-9, both of which were significantly suppressed by subsequent DHA treatment (30 μg/ml, 24 h) (**Figure 5C**). These findings indicate that PV-IgG activates the TLR9/NF-κB pathway and promotes the upregulation of ADAM10 and MMP-9 expression, while DHA mitigates these effects.

DHA mitigated PV-IgG-mediated epidermal blistering and inhibited TLR9/NF-κB activation in vivo

Following PV-IgG administration, mice developed characteristic blistering lesions on the skin surface, while no visible abnormalities were observed in the C-IgG, C-IgG + DHA, or untreated control groups (**Figure 6A**). Histopathological analysis of skin sections confirmed the presence of intraepidermal blisters and acantholytic changes in PV-IgG-treated mice, whereas epidermal integrity remained intact in the control and DHA-treated groups (**Figure 6B**).

IHC staining revealed strong membranous Dsg3 expression in control mice, which was markedly reduced following PV-IgG exposure. Co-treatment with DHA partially restored Dsg3 expression, while no significant difference was observed between the C-IgG and C-IgG + DHA groups (**Figure 6C**). Consistently, IF staining demonstrated that PV-IgG induced Dsg3 internalization and loss of membrane localization,

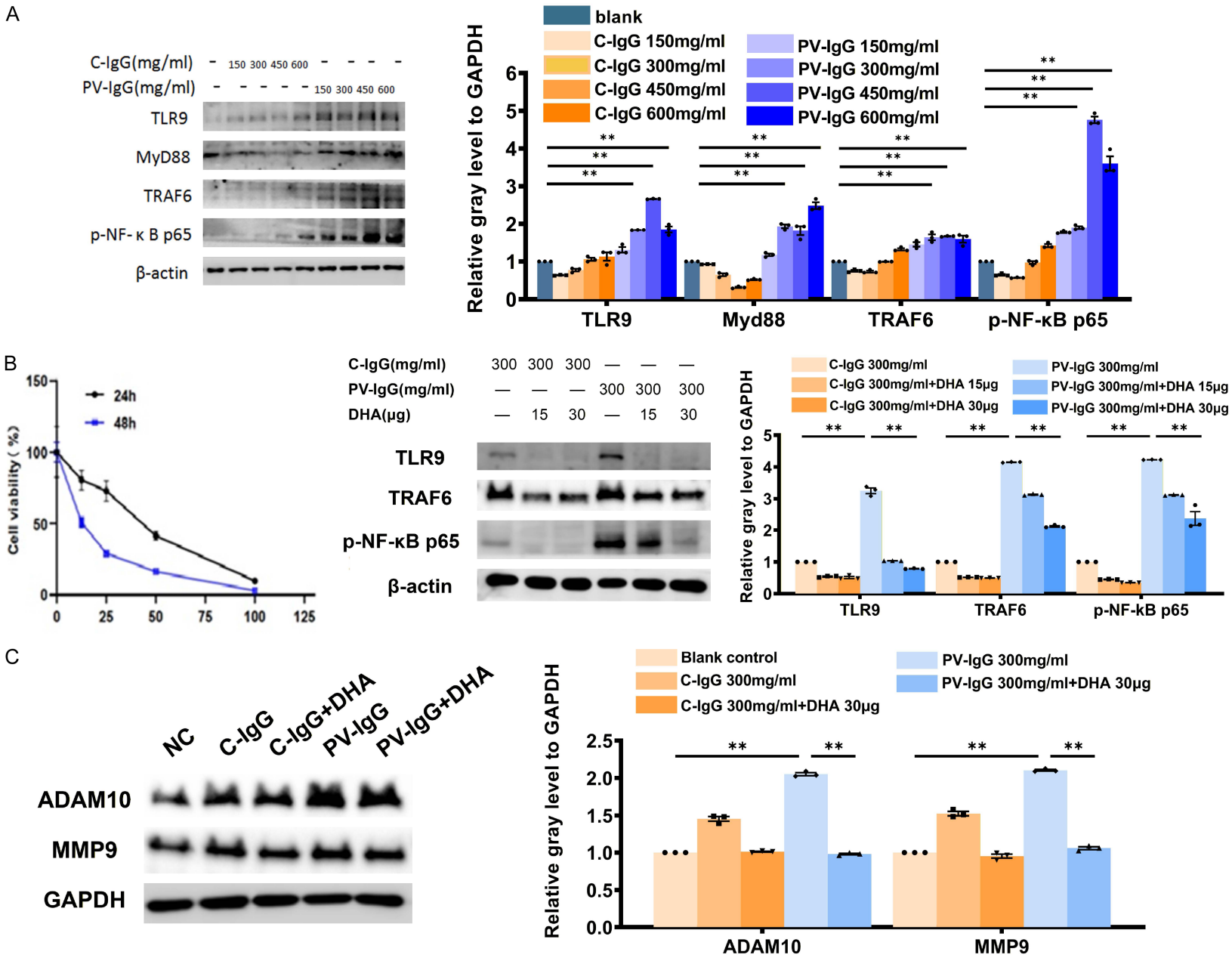
A
C-IgG(mg/ml) - 150 300 450 600 - - - -
PV-IgG(mg/ml) - - - - - 150 300 450 600
TLR9
MyD88
TRAF6
p-NF-κB p65
β-actin
blank
C-IgG 150mg/ml
C-IgG 300mg/ml
C-IgG 450mg/ml
C-IgG 600mg/ml
PV-IgG 150mg/ml
PV-IgG 300mg/ml
PV-IgG 450mg/ml
PV-IgG 600mg/ml
Relative gray level to GAPDH
TLR9
Myd88
TRAF6
p-NF-κB p65
B
Cell viability (%)
24h
48h
C-IgG(mg/ml) 300 300 300 — — —
PV-IgG(mg/ml) — — — 300 300 300
DHA(μg) — 15 30 — 15 30
TLR9
TRAF6
p-NF-κB p65
β-actin
C-IgG 300mg/ml
C-IgG 300mg/ml+DHA 15μg
C-IgG 300mg/ml+DHA 30μg
PV-IgG 300mg/ml
PV-IgG 300mg/ml+DHA 15μg
PV-IgG 300mg/ml+DHA 30μg
Relative gray level to GAPDH
TLR9
TRAF6
p-NF-κB p65
C
NC
C-IgG
C-IgG+DHA
PV-IgG
PV-IgG+DHA
ADAM10
MMP9
GAPDH
Blank control
C-IgG 300mg/ml
C-IgG 300mg/ml+DHA 30μg
PV-IgG 300mg/ml
PV-IgG 300mg/ml+DHA 30μg
Relative gray level to GAPDH
ADAM10
MMP9

Figure 5. DHA attenuated PV-IgG-induced activation of the TLR9/NF-κB signaling pathway in HaCaT keratinocytes. A. Western blot analysis showing concentration-dependent upregulation of TLR9 and its downstream effectors (MyD88, TRAF6, and phosphorylated NF-κB p65) in HaCaT cells treated with PV-IgG; B. DHA exhibited concentration- and time-dependent cytotoxicity and suppressed PV-IgG-induced activation of the TLR9/NF-κB pathway; C. DHA treatment significantly reduced PV-IgG-induced protein expression of ADAM10 and MMP-9. Notes: DHA, dihydroartemisinin; PV, pemphigus vulgaris; $^{**}P < 0.05$.

whereas DHA effectively preserved both expression and membrane distribution of Dsg3 (**Figure 6D**).

In line with the *in vitro* findings, Western blot analysis showed that PV-IgG treatment significantly increased the protein levels of TLR9, TRAF6, phosphorylated NF-κB p65, ADAM10, and MMP-9 compared with the C-IgG group. These elevations were substantially reduced following DHA treatment ($P < 0.05$), indicating that DHA effectively inhibited PV-IgG-induced activation of the TLR9/NF-κB signaling pathway *in vivo* (**Figure 6E**).

Discussion

Pemphigus vulgaris (PV) is a chronic, life-threatening autoimmune blistering disease characterized by the formation of intraepidermal clefts, accompanied by acantholysis [1]. Adjacent keratinocytes are held together by desmosomes, which is essential for skin integrity. In PV, the production of pathogenic IgG autoantibodies, which directly act against Dsg1 and Dsg3 - key components of desmosomes, leads to acantholysis and subsequent blister formation [6, 21]. The expression patterns of Dsg1 and Dsg3 vary across different epithelial sites. In mucosal epithelium, both Dsg1 and Dsg3 are expressed throughout the whole squamous layer, with Dsg3 levels significantly higher than Dsg1. In contrast, in the skin, Dsg1 is expressed more abundantly in the superficial layers, whereas Dsg3 is almost exclusively expressed in the parabasal and basal cell layers [6]. It is widely accepted that the clinical phenotype of PV is determined by the specific desmoglein(s) targeted by autoantibodies. Patients with mucosal-predominant PV predominantly exhibit anti-Dsg3 autoantibodies, whereas the mucocutaneous or cutaneous PV harbor both anti-Dsg3 and anti-Dsg1 autoantibodies [1, 22]. In most PV cases, serum anti-Dsg antibody levels are closely related to disease activity [1].

Accumulating evidence indicates that PV autoantibodies induce blister formation through multiple, non-mutually exclusive mechanisms: (1) autoantibodies directly interference with Dsg trans-interactions through steric hindrance; (2) remodeling of Dsg expression on the cell surface leads to the internalization and depletion of Dsg3 from the cell membrane; (3) signaling activation, including EGFR, p38 mitogen-activated protein kinase (MAPK), MYC proto-oncogene, Rho GTPase, and caspase pathways, disrupt cytoskeletal architecture [6, 23-30]. In addition, autoreactive T and B lymphocytes also play an important role in the pathogenesis of PV. T lymphocytes are mainly divided into $CD4^+$ and $CD8^+$ T cells. The $CD4^+$ autoreactive T lymphocyte specific for Dsg molecules contribute to disease progression by producing IL-10 and by driving B cells to produce Dsg-specific antibodies [6, 27, 31].

Network pharmacology integrates network analysis, systems biology, pleiotropy, and connectivity to elucidate complex drug-target-disease interactions, thereby facilitating drug discovery [32]. By leveraging multi-compound synergy and drug repurposing approaches, network pharmacology facilitates the identification of effective therapeutic interventions while accelerating clinical translation and reducing the need for *de novo* drug development [33]. Based on our results of network pharmacology analysis, the TLR9/NF-kB pathway, which is involved in inflammatory response, immune response, B-cell activation, proliferation and differentiation, was selected for subsequent investigation.

Toll-like receptors (TLRs) play an important role in innate immunity defense against infection and are referred to as pattern recognition receptors [34]. In addition to recognizing exogenous microbial ligands, TLRs also recognize endogenous ligands released by stressed or injured host cells [35]. A total of 10 TLR isoforms have been identified in humans to date, among which TLR2, 4, and 5 are expressed on

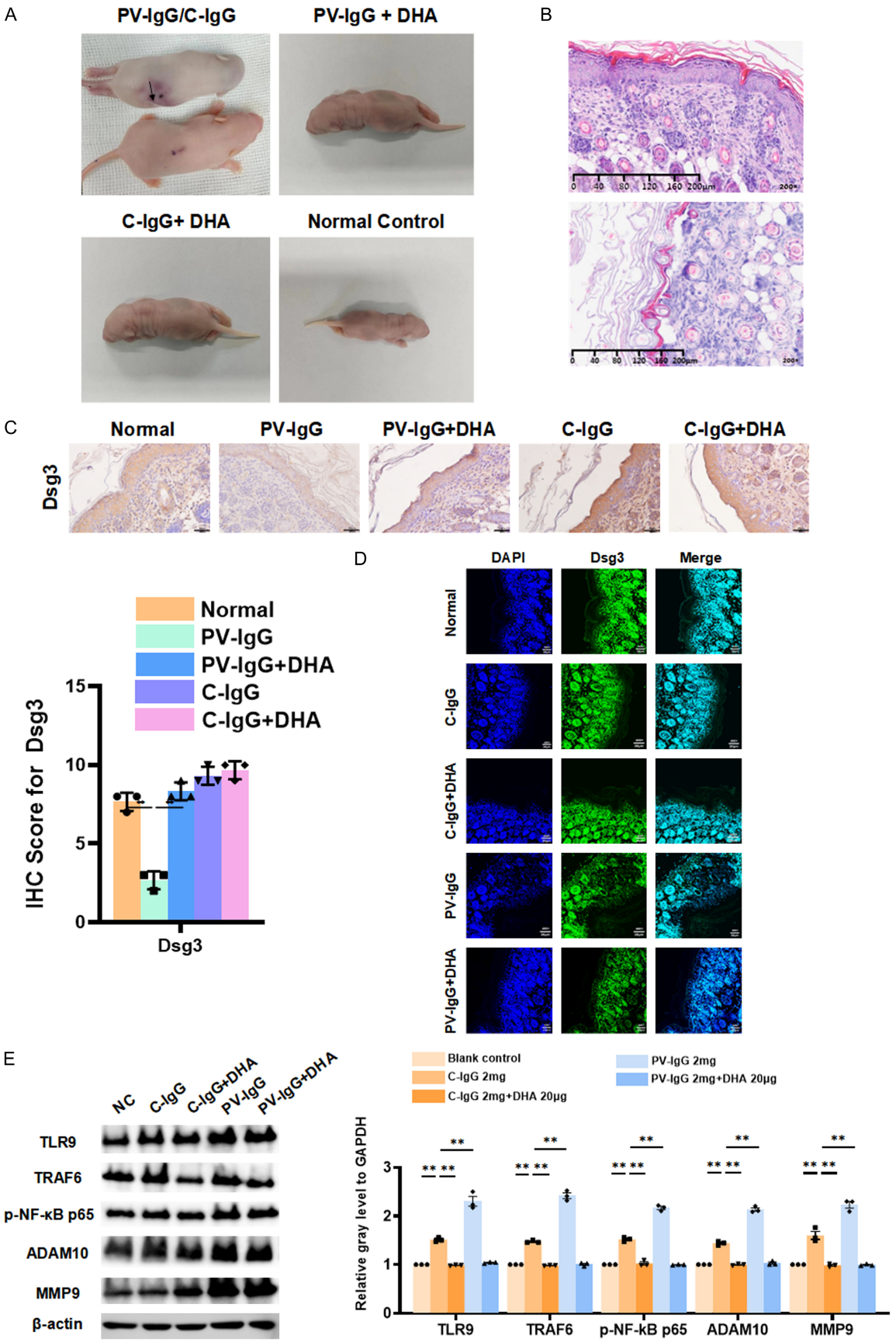
A
PV-IgG/C-IgG
PV-IgG + DHA
C-IgG+ DHA
Normal Control
B
C
Normal
PV-IgG
PV-IgG+DHA
C-IgG
C-IgG+DHA
Dsg3
Normal
PV-IgG
PV-IgG+DHA
C-IgG
C-IgG+DHA
IHC Score for Dsg3
Dsg3
D
DAPI
Dsg3
Merge
Normal
C-IgG
C-IgG+DHA
PV-IgG
PV-IgG+DHA
E
NC
C-IgG
C-IgG+DHA
PV-IgG
PV-IgG+DHA
TLR9
TRAF6
p-NF-κB p65
ADAM10
MMP9
β-actin
Blank control
C-IgG 2mg
C-IgG 2mg+DHA 20μg
PV-IgG 2mg
PV-IgG 2mg+DHA 20μg
Relative gray level to GAPDH
TLR9
TRAF6
p-NF-κB p65
ADAM10
MMP9

Figure 6. DHA mitigated PV-IgG-induced blister formation and restored Dsg3 expression *in vivo*. A. Representative images of mice from different experimental groups: PV-IgG-treated mice exhibiting characteristic blistering lesions (black arrows), PV-IgG + DHA - treated mice showing markedly reduced lesions, and corresponding C-IgG, C-IgG + DHA, and untreated normal controls without visible blisters; B. H&E staining of murine skin sections demonstrating intact epidermal architecture in controls and extensive intraepidermal blistering with acantholysis in PV-IgG-treated mice; C. Immunohistochemical analysis of Dsg3 expression showing strong membranous localization in controls, markedly decreased staining after PV-IgG treatment, and partial restoration following DHA co-administration (n = 3); D. Immunofluorescence analysis confirming that PV-IgG challenge disrupted Dsg3 membrane localization, which was effectively preserved by DHA treatment (×400). E. Western blot analysis of murine skin lysates indicating that PV-IgG increased the expression of TLR9, TRAF6, phosphorylated NF-κB p65, ADAM10, and MMP-9, whereas DHA treatment reversed these changes. Notes: DHA, dihydroartemisinin; PV, pemphigus vulgaris; **P < 0.05.

the cell membrane, whereas TLR3, 7, 8, and 9 are expressed in endosomal compartments [36]. Evidence suggests that TLR3, 4, 9 may be involved in the pathogenesis of PV [37]. TLR9 is known to specifically recognize CpG DNA [38]. Besides that, the autoantibody-autoantigen immune complexes can stimulate endocytosis of bound antigens to facilitate the delivery of chromatin fragments to endosomes, thereby activating TLR9 [39]. From the perspective of molecular function, TLR9 activation represents a crucial initiating link in the inflammatory cascade of PV. PV-IgG binds Dsg3 on the keratinocyte surface and undergoes internalization together with the engaged desmosomal complexes. Previous work has demonstrated that IgG - autoantigen immune complexes can promote endocytosis of associated chromatin or DNA-containing fragments, thereby delivering endogenous nucleic acids into endosomal compartments. Endosomal nucleic acids are canonical ligands for TLR9, which recognizes unmethylated CpG-rich DNA. Thus, PV-IgG may not activate TLR9 by itself, but rather by facilitating the delivery of endogenous DNA-containing material to endosomal TLR9, leading to downstream MyD88-TRAF6-NF-κB activation. This mechanism provides a biologically plausible explanation for our observation that PV-IgG increases TLR9 pathway activity. Nevertheless, our current study establishes correlation rather than direct causality. Future investigations employing pathway blockade, endosomal acidification blockade, and visualization of PV-IgG trafficking into TLR9-positive compartments will be required to determine whether PV-IgG activates TLR9 directly, indirectly, or through DNA-containing immune complexes. Moreover, the downstream cellular signal transduction of TLR9 is strictly dependent on the adaptor protein MyD88 [40]. Activation of MyD88 subsequently recruits interleukin-1 receptor-associated kinases (IRAKs) and TRAF6, ultimately leading to NF-κB activation [38]. In mammalian cells, NF-κB has five member families, namely RelA (p65), RelB, c-Rel, p105/p50 (NF-κB1), and p100/p52 (NF-κB2) [41]. In most cells, NF-κB resides in the cytoplasm as an inactive, latent, IκB-binding complex [42]. For instance, the classical p65:p50 heterodimer is mainly regulated by IκBα [43]. Activated MyD88 recruits TRAF6 and IRAK family members, causing the oligomerization and self-ubiquitination of TRAF6, which in turn activates TAK1. Activated TAK1 may directly phosphorylate IKKβ and activate the IKK complex, leading to IκBα degradation and subsequent NF-κB activation [44]. Degraded IκBα induces nuclear translocation of p65:p50 dimer, as well as phosphorylates p65 TADs to enhance its transcriptional activity and nuclear turnover [43, 45]. P65 can be phosphorylated at multiple residues, including Ser536, Ser529 and Ser276, among which Ser-536 is considered the most critical [41, 46]. Collectively, the NF-κB pathway is activated to regulate innate and adaptive immunity and inflammatory responses [47].

It has been reported that MMP-9 is a downstream molecule of TLR9 signaling, possibly mediated through NF-κB [48-51]. The expression of ADAM10 is likewise regulated by the NF-κB pathway [52]. Both MMP-9 and ADAM10 play critical roles in the pathogenesis of PV [53-56].

DHA enhances cellular immune responses through phosphorylation of MAPK and cyclin-dependent kinase (CDK) to selectively induce the expansion of T-cell subsets and beneficially modulate the host immune system [57]. Besides, DHA can directly inhibit B-cell activation, differentiation, and antibody production [58]. DHA also mitigates inflammatory responses by suppressing TLR4-dependent NF-κB activation [59, 60] and reducing the expression of pro-

inflammatory cytokines, including IL-6 and Il-1β [61].

Conclusion

Our findings suggest that PV-IgG activates NF-κB signaling through TLR9/TRAF6 axis, which can be partially inhibited by DHA. Additionally, DHA effectively suppresses PV-IgG-induced internalization and depletion of Dsg3 and downregulates the expression of ADAM10 and MMP-9, two key mediators involved in the pathogenesis of PV.

Acknowledgements

This work was supported by the Medical Science Research Project of Hebei (No. 20260582) and the Natural Science Foundation of Hebei Province (Grant No. H2022206318).

Disclosure of conflict of interest

None.

Address correspondence to: Wenqing Wang, Department of Dermatology, The Fourth Hospital of Hebei Medical University, No. 12, Jiankang Road, Shijiazhuang, Hebei, China. E-mail: 46700592@hebmu.edu.cn

References

[1] Schmidt E, Kasperkiewicz M and Joly P. Pemphigus. Lancet 2019; 394: 882-894.

[2] Porro AM, Hans Filho G and Santi CG. Consensus on the treatment of autoimmune bullous dermatoses: pemphigus vulgaris and pemphigus foliaceus - Brazilian Society of Dermatology. An Bras Dermatol 2019; 94: 20-32.

[3] Dermatology Branch of China International Exchange and Promotion Association for Medical and Healthcare. Diagnosis and treatment of pemphigus vulgaris: an expert proposal (2020). Chin J Dermatol 2020; 53: 1-7.

[4] Hübner F, Recke A, Zillikens D, Linder R and Schmidt E. Prevalence and age distribution of pemphigus and pemphigoid diseases in Germany. J Invest Dermatol 2016; 136: 2495-2498.

[5] Zhao L, Chen Y and Wang M. The global incidence rate of pemphigus vulgaris: a systematic review and meta-analysis. Dermatology 2023; 239: 514-522.

[6] Kasperkiewicz M, Ellebrecht CT, Takahashi H, Yamagami J, Zillikens D, Payne AS and Amagai M. Pemphigus. Nat Rev Dis Primers 2017; 3: 17026.

[7] Murrell DF, Peña S, Joly P, Marinovic B, Hashimoto T, Diaz LA, Sinha AA, Payne AS, Daneshpazhooh M, Eming R, Jonkman MF, Mimouni D, Borradori L, Kim SC, Yamagami J, Lehman JS, Saleh MA, Culton DA, Czernik A, Zone JJ, Fivenson D, Ujiie H, Wozniak K, Akman-Karakaş A, Bernard P, Korman NJ, Caux F, Drenovska K, Prost-Squarcioni C, Vassileva S, Feldman RJ, Cardones AR, Bauer J, Ioannides D, Jedlickova H, Palisson F, Patsatsi A, Uzun S, Yayli S, Zillikens D, Amagai M, Hertl M, Schmidt E, Aoki V, Grando SA, Shimizu H, Baum S, Cianchini G, Feliciani C, Iranzo P, Mascaró JM Jr, Kowalewski C, Hall R, Groves R, Harman KE, Marinkovich MP, Maverakis E and Werth VP. Diagnosis and management of pemphigus: recommendations of an international panel of expert. J Am Acad Dermatol 2020; 82: 575-585.

[8] Dodiuk-Gad RP, Ish-Shalom S and Shear NH. Systemic glucocorticoids: important issues and practical guidelines for the dermatologist. Int J Dermatol 2015; 54: 723-729.

[9] Tedbirt B, Gillibert A, Andrieu E, Hébert V, Bastos S, Korman NJ, Tang MBY, Li J, Borradori L, Cortés B, Kim SC, Gual A, Xiao T, Wieland CN, Fairley JA, Ezzedine K and Joly P. Mixed individual-aggregate data on all-cause mortality in bullous pemphigoid a meta-analysis. JAMA Dermatol 2021; 157: 421-430.

[10] Hasanaj A, Zaki F, Harman KE, Grindlay D and Gran S. Cause-specific mortality in people with bullous pemphigoid and pemphigus vulgaris: a systematic review and meta-analysis. Br J Dermatol 2022; 186: 359-361.

[11] Tu Y. The discovery of artemisinin (qinghaosu) and gifts from Chinese medicine. Nat Med 2011; 17: 1217-1220.

[12] Tu Y. Artemisinin-a gift from traditional Chinese medicine to the world (Nobel Lecture). Angew Chem Int Ed Engl 2016; 55: 10210-10226.

[13] Morris CA, Duparc S, Borghini-Fuhrer I, Jung D, Shin CS and Fleckenstein L. Review of the clinical pharmacokinetics of artesunate and its active metabolite dihydroartemisin in following intravenous, intramuscular, oral or rectal administration. Malar J 2011; 10: 263.

[14] Li WD, Dong YJ, Tu YY and Lin ZB. Dihydroarteannuin ameliorates lupus symptom of BXSB mice by inhibiting production of TNF-alpha and blocking the signaling pathway NF-kappa B translocation. Int Immunopharmacol 2006; 6: 1243-1250.

[15] Chen Y, Yan Y, Liu H, Qiu F, Liang CL, Zhang Q, Huang RY, Han L, Lu C and Dai Z. Dihydroartemisinin ameliorates psoriatic skin inflammation and its relapse by diminishing $CD8^+$ T-cellmemory in wild-type and humanized mice. Theranostics 2020; 10: 10466-10482.

[16] Zhao YG, Wang Y, Guo Z, Gu AD, Dan HC, Baldwin AS, Hao W and Wan YY. Dihydroartemisinin ameliorates inflammatory disease by its reciprocal effects on Th and regulatory T cell function via modulating the mammalian target of rapamycin pathway. J Immunol 2012; 189: 4417-4425.
[17] Wei M, Xie X, Chu X, Yang X, Guan M and Wang D. Dihydroartemisinin suppresses ovalbumin-induced airway inflammation in a mouse allergicasthma model. Immunopharmacol Immunotoxicol 2013; 35: 382-389.
[18] Liu H, Tian Q, Ai X, Qin Y, Cui Z, Li M, Yang J, Zhai D, Liu Y, Chen S, Meng J, Sun T, Zhou H and Yang C. Dihydroartemisinin attenuates autoimmune thyroiditis by inhibiting the CXCR3/PI3K/AKT/NF-κB signaling pathway. Oncotarget 2017; 8: 115028-115040.
[19] Fan M, Li Y, Yao C, Liu X, Liu X and Liu J. Dihydroartemisinin derivative DC32 attenuates collagen-induced arthritis in mice by restoring the Treg/Th17 balance and inhibiting synovitis through down-regulation of IL-6. Int Immunopharmacol 2018; 65: 233-243.
[20] China Dermatologist Association. Guidelines for diagnosis and treatment of pemphigus in China (2024). Chin J Dermatol 2024; 57: 873-886.
[21] Kayani M and Aslam AM. Bullous pemphigoid and pemphigus vulgaris. BMJ 2017; 357: j2169.
[22] Koga H, Tsuruta D, Ohyama B, Ishii N, Hamada T, Ohata C, Furumura M and Hashimoto T. Desmoglein 3, its pathogenicity and a possibility for therapeutic target in pemphigus vulgaris. Expert Opin Ther Targets 2013; 17: 293-306.
[23] Diercks GF, Pas HH and Jonkman MF. The ultrastructure of acantholysis in pemphigus vulgaris. Br J Dermatol 2009; 160: 460-461.
[24] Jennings JM, Tucker DK, Kottke MD, Saito M, Delva E, Hanakawa Y, Amagai M and Kowalczyk AP. Desmosome disassembly in response to pemphigus vulgaris IgG occurs in distinct phases and can be reversed by expression of exogenous Dsg3. J Invest Dermatol 2011; 131: 706-718.
[25] Ke J and Spindler V. Desmosomes and extra desmosomal adhesive signaling contacts in pemphigus. Med Res Rev 2014; 34: 1127-1145.
[26] Spindler V, Eming R, Schmidt E, Amagai M, Grando S, Jonkman MF, Kowalczyk AP, Müller EJ, Payne AS, Pincelli C, Sinha AA, Sprecher E, Zillikens D, Hertl M and Waschke J. Mechanisms causing loss of Keratinocyte Cohesion in Pemphigus. J Invest Dermatol 2018; 138: 32-37.
[27] Pollmann R, Schmidt T, Eming R and Hertl M. Pemphigus: a comprehensive review on pathogenesis, clinical presentation and novel therapeutic approaches. Clin Rev Allergy Immunol 2018; 54: 1-25.
[28] Hammers CM and Stanley JR. Mechanisms of disease: pemphigus and bullous pemphigoid. Annu Rev Pathol 2016; 11: 175-197.
[29] Schlögl E, Radeva MY, Vielmuth F, Schinner C, Waschke J and Spindler V. Keratin retraction and desmoglein3 internalization independently contribute to autoantibody-induced cell dissociation in pemphigus vulgaris. Front Immunol 2018; 9: 858.
[30] Delva E, Jennings JM, Calkins CC, Kottke MD, Faundez V and Kowalczyk AP. Pemphigus vulgaris IgG-induced desmoglein-3 endocytosis and desmosomal disassembly are mediated by a clathrin-and dynamin-independent mechanism. J Biol Chem 2008; 283: 18303-18313.
[31] Hertl M, Eming R and Veldman C. T cell control in autoimmune bullous skin disorders. J Clin Invest 2006; 116: 1159-1166.
[32] Hopkins AL. Network pharmacology: the next paradigm in drug discovery. Nat Chem Biol 2008; 4: 682-690.
[33] Nogales C, Mamdouh ZM, List M, Kiel C, Casas AI and Schmidt HHHW. Network pharmacology: curing causal mechanisms instead of treating symptoms. Trends Pharmacol Sci 2022; 43: 136-150.
[34] Kang JY and Lee JO. Structural biology of the toll-like receptor family. Annu Rev Biochem 2011; 80: 917-941.
[35] Li M, Carpio DF, Zheng Y, Bruzzo P, Singh V, Ouaaz F, Medzhitov RM and Beg AA. An essential role of the NF-kappa B/Toll-like receptor pathway in induction of inflammatory and tissue-repair gene expression by necrotic cells. J Immunol 2001; 166: 7128-7135.
[36] Wagner H. The immunobiology of the TLR9 subfamily. Trends Immunol 2004; 25: 381-386.
[37] Gao C, Liu M, Xin Y, Zeng Y, Yang H, Fan X, Zhao C, Zhang B, Zhang L, Li JJ, Zhao M, Wang Z and Lu Q. Immunostimulatory effects of Toll-like receptor ligands as adjuvants in establishing a novel mouse model for pemphigus vulgaris. Clin Transl Med 2024; 14: e1765.
[38] Takeda K, Kaisho T and Akira S. Toll-like receptors. Annu Rev Immunol 2003; 21: 335-376.
[39] Leadbetter EA, Rifkin IR, Hohlbaum AM, Beaudette BC, Shlomchik MJ and Marshak-Rothstein A. Chromatin-IgG complexes activate B cells by dual engagement of IgM and Toll-like receptors. Nature 2002; 416: 603-607.
[40] Ishii KJ and Akira S. Innate immune recognition of, and regulation by, DNA. Trends Immunol 2006; 27: 525-532.
[41] Bakkar N and Guttridge DC. NF-kappaB signaling: a tale of two pathways in skeletal myogenesis. Physiol Rev 2010; 90: 495-511.

[42] Gilmore TD. Introduction to NF-κB: players, pathways, perspectives. Oncogene 2006; 25: 6680-6684.
[43] Karin M and Ben-Neriah Y. Phosphorylation meets ubiquitination: the control of NF-[kappa] B activity. Annu Rev Immunol 2000; 18: 621-663.
[44] Vallabhapurapu S and Karin M. Regulation and function of NF-κB transcription factors in the immune system. Annu Rev Immunol 2009; 27: 693-733.
[45] Lawrence T, Bebien M, Liu GY, Nizet V and Karin M. IKKalpha limits macrophage NF-kappaB activation and contributes to the resolution of inflammation. Nature 2005; 434: 1138-1143.
[46] Sakurai H, Chiba H, Miyoshi H, Sugita T and Toriumi W. IkappaB kinases phosphorylate NF-kappaB p65 subunit on serine 536 in the transactivation domain. J Biol Chem 1999; 274: 30353-30356.
[47] Li Q and Verma IM. NF-kappaB regulation in the immune system. Nat Rev Immunol 2002; 2: 725-734.
[48] Jing Y, Jia M, Zhuang J, Han D, Zhou C and Yan J. TLR9 exerts an oncogenic role in promoting osteosarcoma progression depending on the regulation of NF-κB signaling pathway. Biol Pharm Bull 2022; 45: 1733-1742.
[49] Merrell MA, Ilvesaro JM, Lehtonen N, Sorsa T, Gehrs B, Rosenthal E, Chen D, Shackley B, Harris KW and Selander KS. Toll-like receptor 9 agonists promote cellular invasion by increasing matrix metalloproteinase activity. Mol Cancer Res 2006; 4: 437-447.
[50] Shin EM, Hay HS, Lee MH, Goh JN, Tan TZ, Sen YP, Lim SW, Yousef EM, Ong HT, Thike AA, Kong X, Wu Z, Mendoz E, Sun W, Salto-Tellez M, Lim CT, Lobie PE, Lim YP, Yap CT, Zeng Q, Sethi G, Lee MB, Tan P, Goh BC, Miller LD, Thiery JP, Zhu T, Gaboury L, Tan PH, Hui KM, Yip GW, Miyamoto S, Kumar AP and Tergaonkar V. DEAD-box helicase DP103 defines metastatic potential of human breast cancers. J Clin Invest 2014; 124: 3807-3824.
[51] Hasan MK, Widhopf Ii GF, Ghia EM and Kipps TJ. Wnt5a induces ROR1 dependent NF-κB activation to enhance MMP-9 expression and invasiveness in chronic lymphocytic leukemia. Leukemia 2025; 39: 1661-1669.
[52] Gao JH, He AD, Liu LM, Zhou YJ, Guo YW, Lu M, Zeng XB, Gong X, Lu YJ, Liang HF, Zhang BX, Ma R, Zhang RY and Ming ZY. Direct interaction of platelet with tumor cell aggravates hepatocellular carcinoma metastasis by activating TLR4/ADAM10/CX3CL1 axis. Cancer Lett 2024; 585: 216674.
[53] Chen Y, Wang YF, Song SS, Zhu J, Wu LL and Li XY. Potential shared therapeutic and hepatotoxic mechanisms of Tripterygium wilfordii polyglycosides treating three kinds of autoimmune skin diseases by regulating IL-17 signaling pathway and Th17 cell differentiation. J Ethnopharmacol 2022; 296: 115496.
[54] Ivars M, España A, Alzuguren P, Pelacho B, Lasarte JJ and López-Zabalza MJ. The involvement of ADAM10 in acantholysis in mucocutaneous pemphigus vulgaris depends on the autoantibody profile of each patient. Br J Dermatol 2020; 182: 1194-1204.
[55] Kugelmann D, Anders M, Sigmund AM, Egu DT, Eichkorn RA, Yazdi AS, Sárdy M, Hertl M, Didona D, Hashimoto T and Waschke J. Role of ADAM10 and ADAM17 in the regulation of keratinocyte adhesion in pemphigus vulgaris. Front Immunol 2022; 13: 884248.
[56] Cirillo N and Prime SS. A scoping review of the role of metalloproteinases in the pathogenesis of autoimmune pemphigus and pemphigoid. Biomolecules 2021; 11: 1506.
[57] Li Q, Yuan Q, Jiang N, Zhang Y, Su Z, Lv L, Sang X, Chen R, Feng Y and Chen Q. Dihydroartemisinin regulates immune cell heterogeneity by triggering a cascade reaction of CDK and MAPK phosphorylation. Signal Transduct Target Ther 2022; 7: 222.
[58] Shi X, Liao T, Chen Y, Chen J, Liu Y, Zhao J, Dang J, Sun Q and Pan Y. Dihydroartemisinin inhibits follicular helper T and B cells: implications for systemic lupus erythematosus treatment. Arch Pharm Res 2024; 47: 632-644.
[59] Ji Y, Sun K, Yang Y and Wu Z. Dihydroartemisinin ameliorates innate inflammatory response induced by Streptococcussuis-derived muramidase-released protein via inactivation of TLR4-dependent NF-κB signaling. J Pharm Anal 2023; 13: 1183-1194.
[60] Liu X, Lu J, Liao Y, Liu S, Chen Y, He R, Men L, Lu C, Chen Z, Li S, Xiong G and Yang S. Dihydroartemisinin attenuates lipopolysaccharide-induced acute kidney injury by inhibiting inflammation and oxidative stress. Biomed Pharmacother 2019; 117: 109070.
[61] Yin J, Xia W, Zhang Y, Ding G, Chen L, Yang G, Huang S, Jia Z and Zhang A. Role of dihydroartemisinin in regulating prostaglandin E_2 synthesis cascade and inflammation in endothelial cells. Heart Vessels 2018; 33: 1411-1422.